

RESEARCH

Open Access



# Optimization and characterization of quercetin-loaded solid lipid nanoparticles for biomedical application in colorectal cancer

Jamal Moideen Muthu Mohamed<sup>1</sup>, Fazil Ahmad<sup>2</sup>, Mohamed El-Sherbiny<sup>3,4</sup>, Mohammed Ahmad Al Mohaini<sup>5,6</sup>, Krishnaraju Venkatesan<sup>7</sup>, Yahya Bin Abdullah Alrashdi<sup>8</sup>, Mamdouh Basheir Eldesoqi<sup>3,6</sup>, Adel Ehab Ibrahim<sup>9</sup>, Amal Fahmy Dawood<sup>10</sup>, Ateya Megahed Ibrahim<sup>11,12</sup> and Sami El Deeb<sup>13\*</sup>

\*Correspondence:  
s.eldeeb@tu-bs.de

<sup>13</sup> Institute of Medicinal and Pharmaceutical Chemistry, Technische Universitaet Braunschweig, Braunschweig, Germany  
Full list of author information is available at the end of the article

## Abstract

**Background:** Colorectal cancer (CRC) is a type of cancer that affects the colon or rectum and occurs in individuals over the age of 50, although it can affect people of all ages. Quercetin is a flavonoid, which is a type of plant pigment with antioxidant and anti-inflammatory properties. Some studies have explored the potential of quercetin as an adjuvant therapy to enhance the effectiveness of chemotherapy or radiation therapy.

**Methodology:** In the proposed work, the nano-biomaterials of solid lipids such as stearic acid (SA) and tripalmitin (TpN) as well as the surfactants tween 80 and span 80 were used to prepare novel quercetin (QuR)-loaded-solid lipid nanoparticles (QuR-SLNs) for medical applications in colorectal cancer (CRC). The resulting bio-nano SLNs' mean entrapment efficiency (EE) and particle size (PS) were optimized by Box–Behnken design (BBD) approach based on the response-like surface methodology (RSM). The variables include lipid ratio ( $X_1$ ), surfactant ratio ( $X_2$ ), QuR-to-lipid ratio ( $X_3$ ), the sonication time ( $X_4$ ), and the homogenization time ( $X_5$ ). Requirements on the maximum EE (%) and minimum PS (nm) were optimized for the preparation of QuR-SLN. Differential scanning calorimetry (DSC), X-ray diffraction (XRD) analysis, and scanning electron microscopy (SEM) were then used to analyze the optimized SLN and to find the crystalline state of QuR with lipid relationship. In addition, on the Caco-2 cells, at  $IC_{50}$  (49  $\mu$ M/mL), in vitro cytotoxicity was attained.

**Results:** The optimized QuR-SLN had practically spherical shapes, with % EE and a PS of  $97.8 \pm 1.16\%$  and  $132.16 \pm 4.1$  nm, respectively. In aqueous media, the degree of lipid crystallinity and the lipid modification was investigated, and the QuR incorporation and release patterns showed high correlations with both. The results showed that over  $41.12 \pm 1.6\%$  of the bio-nano QuR-SLNs was released gradually over the course of 48 h, demonstrating effective QuR delayed release. Results on apoptotic observations indicate that apoptosis accounts for the majority of cell death, while necrosis, a type of cell death, constitutes a very minor portion. In conclusion, the prepared bio-nano QuR-SLNs might improve cytotoxicity and can act as an ideal carrier for the delivery of QuR and this preparation is used in the treatment of CRC.



**Keywords:** Ultrasonication, Quercetin, MTT assay, Box–Behnken design, Anticancer, Solid lipid nanoparticles

## Introduction

One of the most prevalent types of gastrointestinal cancer in the world is colorectal cancer (CRC), a malignant tumor which begins in the rectum or colon. Every year, around 150,000 new patients are identified in the USA, and 35% of them will face death from CRC (Rawla et al. 2019). Even though the exact etiology of CRC is unidentified, it is believed to be complex, and mounting data point to a connection between several risk factors and the condition. For instance, there is evidence that lifestyle variables such as nutrition, smoking, and alcohol use, as well as genetic factors such as family history, hereditary disorders, racial and cultural origin, are substantially connected with the development of colon cancer (Mármol et al. 2017).

Various studies suggest that quercetin (QuR) may have anticancer effects, including the ability to inhibit the growth of cancer cells and induce apoptosis (programmed cell death). It has been proposed that quercetin may interfere with various signaling pathways involved in cancer development and progression (Lotfi et al. 2023). QuR (3,3',4',5,7-pentahydroxyflavone) is the most essential member of the flavonol subclass of flavonoids. It has been demonstrated to have a wide range of pharmacological and biological effects on coronary arteries, blood cholesterol levels, platelet aggregation, cancer, oxidative stress, anemia, inflammation, and anaphylaxis (David et al. 2016). There is increased interest in the treatment of cancer due to the positive benefits of chemoprophylaxis and the therapeutic effects of quercetin.

Various factors are essential to be taken into account while selecting QuR-SLNs for anticancer purposes, including the anticancer effects observed in numerous preclinical studies. It is believed to interfere with several cellular processes involved in cancer development, including cell proliferation, apoptosis, and angiogenesis (Michalkova et al. 2023). Also, it has natural flavonoids with a class of polyphenols that are abundantly present in our everyday food and the plant kingdom. In addition, it can reverse multidrug resistance of cancer cells and boost the anticancer effects of another drug (El-Hela et al. 2023).

Although QuR exhibits promising antitumor activity, its therapeutic utility has been limited by its rapid metabolism, low water solubility, stability, and systemic elimination. The poor aqueous solubility of QuR significantly decreases the bioavailability and stability of the pharmaceutical formulations. Various formulations, such as nanoparticles, micelles, or complexes, have been developed to improve the solubility and bioavailability of QuR. Numerous QuR delivery strategies, including liposomes, solid dispersion, phospholipid complexes, polymeric nanoparticles, and nanocrystals, have been researched to overcome these constraints (Das et al. 2020; Roy et al. 2023). These systems have several complications, including drug leakage, poor physical stability, and possible excipient toxicity. A novel nano drug delivery system has emerged, combining the benefits of polymeric nanoparticles and solid lipid nanoparticles (SLNs).

Because of their excellent tolerance and biological degradability, physical–chemical stability, potential for large-scale manufacture, and addition of lipophilic drug into the

lipid structure, solid lipid nanoparticles (SLNs) have gained attention in controlling drug delivery. Well-suited high-melting point lipids make up the core principle of SLNs, while the outer shell is covered with nontoxic amphiphilic surfactants (Jacob et al. 2022). At both room and body temperatures, nanoparticles between 50 and 1000 nm in size are solid, but triglycerides and their mixes, waxes, and fatty acids have an extensive range of applications in SLNs. Lipids along with surfactants and their mixtures are directly proportional to the particle size (PS), which has a significant impact on the physical and chemical properties and stability of the drug-enclosed SLNs. For each drug, an ideal SLN formulation requires consideration of drug loading and release behavior (Muthu Mohamed et al. 2022).

Over the previous several years, research has been carried out on the utilization of QuR as a promising novel natural molecule for cancer treatment and chemoprevention therapy. Although QuR exhibits promising antitumor activity, its therapeutic utility has been limited by its rapid metabolism, low water solubility, stability, and systemic elimination. Numerous QuR delivery strategies, including liposomes, solid dispersion, phospholipid complexes, polymeric nanoparticles, and nanocrystals, have been researched to overcome these constraints. These systems have several problems, including drug leakage, poor physical stability, and possible excipient toxicity. Therefore, SLNs avoid the drawbacks of polymeric nanoparticles and liposomes, which include undesirable stability issues and potential material toxicity, and simultaneously offer stability and biological compatibility of the solid lipid matrix.

In this study, a mixture of stearic acid (SA) and tripalmitin (TpN) was used as the lipid core. Subsequently, a combination of emulsifiers such as Tween 80 and Span 80 was utilized to prepare QuR-loaded solid lipid nanoparticles (QuR-SLNs) (Gao et al. 2013). SLNs were formulated using the micro-emulsion technique. To achieve uniform distribution and lower PS, a combination of ultrasonication and high-speed homogenization is needed. The equipment utilized in these approaches is extremely common in all laboratories, which is one of their biggest advantages. Investigations were conducted on the impacts of surfactant composition and composition of lipid mixture on the PS, EE, thermal properties, and the drug release behavior of delivery systems.

## **Materials and methods**

### **Materials**

The following substances were bought from the Indian market. Quercetin (QuR) from SRL Pvt. Ltd., Maharashtra, India. Free samples provided by Hi-media in Maharashtra, India, are tripalmitin (TpN) and stearic acid (SA). Tween 80 and Span 80 were obtained from Sigma Aldrich, Bengaluru, India. Cell culture: the NCCS (National Center for Cell Science) in Pune provided the colorectal adenocarcinoma cell lines (human) of Caco-2. The cells were sown in DMEM (Sigma-Aldrich, USA), supplemented with FBS (10%), and streptomycin/penicillin as an antibiotic (20 mL, 1%; Hi-media, Mumbai, India), at 37 °C in a humid environment of 5% CO<sub>2</sub> in a CO<sub>2</sub> incubator (Thermo Scientific, USA). Analytical-grade chemicals and reagents were used in this study.

**Preparation of QuR-loaded SLNs (QuR-SLNs)**

The aqueous and oil phases were prepared separately, and QuR-loaded (QuR-SLNs) and QuR-free SLN (blank SLN; B-SLN) were prepared by micro-emulsion method, followed by ultrasonication (Kumar et al. 2018). QuR, TpN, and SA made up the oil phase, while nonionic surfactants (Tween 80 and Span 80) made up the aqueous phase. The two phases were simultaneously heated for 10 min at a separate temperature of 70 °C. The oil phase was added with the aqueous phase before being subjected to sonication at various intervals of time and at 70 °C using a heated ultrasonic bath (Tecno-GAZ SPA Ultra Sonic System) at a rate of 40 to 89 kHz and a power rating of 120 W was employed. The emulsion was then diluted with 25 mL final volume of cold water (2 to 4 °C) with 5 min stirring. The suspension was then homogenized (Ultra Turrax T25, IKA, Ohio, USA) at 12,500 rpm, at various time intervals (to be changed).

**Box–Behnken design (BBD) for screening**

A BBD was facilitated to determine the coefficient of parameters and their influences including the correlation, which were assessed by ANOVA with confidence interval (95%) after executing a limited number of runs and lowering the mistakes and cost (Greenland et al. 2016). The current investigational design has been subjected to several factors, including the ratios of SA to TpN ( $X_1$ ), Span 80 to Tween 80 ( $X_2$ ), QuR to lipid ( $X_3$ ), sonication time ( $X_4$ ), and homogenization time ( $X_5$ ) (Table 1).

To minimize the influence of variables, 46 random trials were selected and optimized using this design. Statistical analysis was based on Fisher’s theory, and the efficacy of the model and the influence of key elements were evaluated using ANOVA. The criteria calculated for each variable (at  $p$ -value < 0.05 and  $F$  value > 0.05) was used to determine the substantial impact of each factor to the model and their significant contribution

**Percentage entrapment efficiency (% EE)**

After passing the aqueous dispersion through a 0.45-m syringe filter, an Agilent Cary 60 UV–Vis spectrophotometer (USA) was used to detect the proportion of integrated QuR (% EE) at 382 nm. After identifying the quantity of untrapped QuR in the filtrate, the quantity of added QuR was considered by deducting the amount of original drug from the amount of free drug (Yadav et al. 2022). Equation (1) was used to determine the drug % EE in the SLNs:

**Table 1** Various independent variables in BBD for the preparation of QuR-SLN

Factors	Levels		
	Low	Center	High
( $X_1$ ) SA/TpN ratio (mg/mg)	25.0	50.0	75.0
( $X_2$ ) Tween 80/Span 80 ratio (S1/S2)	30.0	50.0	70.0
( $X_3$ ) lipid/drug ratio (mg/mg)	2.5	5.0	7.5
( $X_4$ ) sonication time (min)	4.0	5.0	6.0
( $X_5$ ) homogenization time (min)	4.0	5.0	6.0

$$\% EE = \frac{\text{Amount of QuR added in QuR-SLN} - \text{Amount of free QuR}}{\text{Amount of QuR added in QuR-SLN}} \times 100. \quad (1)$$

### In vitro QuR release studies

The dialysis bag (M.W. cutoff: 12,000 Da) method was employed to study the drug release pattern of the ideal preparation of QuR-SLNs, and the dissolution medium was a mixture of 50% ethanol and phosphate buffer (50:50; PBS, pH 6.8) (Satheesh et al. 2022). The dialysis bag was initially packed with 10 mL of prepared QuR-SLN and it was previously being soaked in PBS (pH 6.8) for 12 h. The dissolution media was then added, maintained at 37 °C, and combined while being stirred magnetically (100 rpm). Then, 2 mL of dissolving medium was elevated and substituted with the same quantity of new dissolution media at various times (0.5, 1, 2, 4, 8, 12, 24, and 48 h). According to the established technique, the level of QuR was measured using spectrophotometry at 382 nm. All tests were run in triplicate, and the outcomes were presented as mean  $\pm$  standard deviation.

### Release kinetics from QuR-SLN

Various kinetic release models were used to understand the kinetics of drug release from the preparation, including the Higuchi model (% CDR vs. square root of time), the first order (% log of QuR balance vs. time), and the zero order (% CDR vs. time). The highest regression values were used to make the determination of the ideal functioning and high linear ( $R^2$ ) fitting model.

### Desirability function

After constructing polynomial equations that establish the relationship between both responses to meet the specified variables, they were expressed and judged using the desirability function (DF), which ranges from 0 to 1. In our earlier papers, the phenomena and utility of respective variables were presented in complete detail (Rahman et al. 2019). The BBD technique is more widely used for estimation and evaluation of the key factors and their interactions in an economically efficient pathway, which correlates the numerical pattern of the variables' responses in a quadratic manner (Table 2).

### MTT assay

On Caco-2 cell lines, the MTT (3-[4,5-dimethylthiazol-2-yl]-2,5-diphenyltetrazolium bromide) assay was carried out (Muthu Mohamed et al. 2022). The cells were grown up at a density of  $5 \times 10^4$  cells in 96-well culture plates. The cells were employed as a control using 200  $\mu$ L/well DMSO solvent. Following a 24-h incubation period, the prepared QuR-SLNs were treated with 20  $\mu$ L/well MTT reagent and incubated for an additional 4 h at 37 °C. The 100  $\mu$ L DMSO solvent was added to each well to dilute the purple formazan product. The absorption of the aforementioned solution was estimated with a plate reader (iMark, Bio-Rad, USA) at 570 nm. This statistic was utilized to calculate the inhibition percentage using the following formula:

$$\% \text{ cell inhibition} = \frac{\text{OD control} - \text{OD test}}{\text{OD control}} \times 100. \quad (2)$$

**Table 2** BBD parameters attained for several runs and trial ranges of PS (nm) and EE (%)

Std.	Run	X <sub>1</sub>	X <sub>2</sub>	X <sub>3</sub>	X <sub>4</sub>	X <sub>5</sub>	PS		EE (%)	
							Actual	Predicted	Actual	Predicted
1	1	25	30	5	5	5	129.32	129.98	97.07	97.52
2	2	75	30	5	5	5	238.1	237.70	97.01	97.37
3	5	25	70	5	5	5	131.38	130.81	98.76	98.24
4	7	75	70	5	5	5	177.98	178.49	97.44	97.66
5	20	50	50	2.5	4	5	119.01	119.28	98.31	98.41
6	37	50	50	7.5	4	5	178.98	178.49	97.51	97.66
7	23	50	50	2.5	6	5	227.12	227.00	97.33	97.34
8	11	50	50	7.5	6	5	136.01	136.05	98.14	98.80
9	19	50	30	5	5	4	113.63	113.21	97.09	97.13
10	29	50	70	5	5	4	161.97	162.21	97.89	97.52
11	39	50	30	5	5	6	194.82	196.09	98.67	98.10
12	26	50	70	5	5	6	136.2	134.73	97.56	97.00
13	9	25	50	2.5	5	5	221.76	220.93	98.25	98.11
14	13	75	50	2.5	5	5	179.2	178.49	97.23	97.66
15	8	25	50	7.5	5	5	177.82	178.49	97.11	97.66
16	33	75	50	7.5	5	5	161.56	161.72	97.9	98.10
17	10	50	50	5	4	4	189.67	190.02	97.02	97.57
18	25	50	50	5	6	4	178.78	178.49	97.42	97.66
19	34	50	50	5	4	6	174.02	173.73	97.59	97.40
20	41	50	50	5	6	6	160.71	160.89	98.43	98.34
21	22	50	30	2.5	5	5	115.01	114.52	98.98	98.93
22	16	50	70	2.5	5	5	173.03	172.42	97.5	97.15
23	38	50	30	7.5	5	5	171.95	173.25	97.1	96.90
24	43	50	70	7.5	5	5	176.67	177.18	97.87	98.02
25	31	25	50	5	4	5	175.01	174.57	97.21	97.03
26	35	75	50	5	4	5	183.12	183.25	98.32	98.60
27	3	25	50	5	6	5	243.01	242.46	99.01	99.09
28	44	75	50	5	6	5	200.1	200.02	98.22	98.07
29	42	50	50	2.5	5	4	163.02	163.04	97.11	97.15
30	36	50	50	7.5	5	4	179	178.49	97.66	97.66
31	24	50	50	2.5	5	6	117.91	118.45	97.47	97.69
32	28	50	50	7.5	5	6	180.1	179.32	97.32	97.43
33	21	25	50	5	5	4	244.13	243.77	96.11	96.59
34	45	75	50	5	5	4	181.71	182.42	98.3	98.12
35	12	25	50	5	5	6	225.91	226.17	98.1	97.94
36	27	75	50	5	5	6	179.63	179.81	97.55	97.32
37	40	50	30	5	4	5	184.01	183.73	97.76	97.30
38	46	50	70	5	4	5	195.21	195.26	98.05	97.74
39	17	50	30	5	6	5	193.89	193.94	97.43	97.48
40	32	50	70	5	6	5	177.58	177.66	97.43	97.32
41	6	50	50	5	5	5	194.42	194.78	97.96	97.97
42	4	50	50	5	5	5	156.55	156.97	97.16	97.22
43	15	50	50	5	5	5	184.67	184.56	97.42	97.66
44	18	50	50	5	5	5	237.99	238.53	97.66	96.76
45	14	50	50	5	5	5	222.23	222.25	95.01	95.61
46	30	50	50	5	5	5	166.66	166.96	98.87	98.32

It would yield the  $IC_{50}$  concentration, which will be determined from the MTT experiment, to kill 50% of the cells.

### **Apoptosis study**

#### ***Acridine orange (AO)/ethidium bromide (EB) stain***

Six-well culture plates with  $5 \times 10^4$  Caco-2 cells were then seeded and permitted to grow to 80% gathering. Following that, QuR-SLN was added to the cells and cultured for 24 h at their  $IC_{50}$  concentration (determined by the MTT assay; it has produced the highest results in the MTT assay). The cells were trypsinized and suspended in phosphate-buffered saline (PBS). A droplet of cell suspension was applied to a glass slide and mixed with AO/EB (25  $\mu$ L containing 3.8  $\mu$ M of AO and 2.5  $\mu$ M of EB in PBS) before being covered through a cover slip. The colored cells were magnified by 400 $\times$  using a Carl Zeiss fluorescent microscope (Jena, Germany) committed with a range of UV-filter at 450–490 nm. The number of cells that had destructive changes was determined.

#### ***Hoechst stain***

After trypsinization, the cell suspension was stained with Hoechst 33258 dye and hatched at 37 °C for 15 min (Mohamed et al. 2021a, b). The cells were previously assessed for the proportion of cells with pathogenic alterations using a fluorescence microscope at a magnification of 400 $\times$ .

### **Statistical analysis**

Data were calculated using mean and standard deviation (mean  $\pm$  SD). Student's *t* test and one-way ANOVA analysis results were used to express the difference in statistically significant values. Statistical significance was defined as a *p*-value of 0.05 or below.

## **Results and discussion**

### **Data from an experiment statistically analyzed by Design-Expert software**

The outcomes of 46 investigational runs using Box–Behnken designs together with their two answers are illustrated in Table 2. The obtained results from analysis of variance (ANOVA) were based on Fischer tests, which calculated the probability values (*p*-value) for PS and % EE at 95% confidence level. The lack of fit (LOF), which represents the data fluctuation about the fitted model, serves as a standard for determining whether a model is adequate for fitting an investigational outcome. The lack of significance in the LOF value demonstrates the model's appropriateness for being accurately suitable with the experimental data. The LOF's *p*-values for PS and % EE, respectively, were 0.79 and 0.98, both of which demonstrate the high level of significance and possible use in determining the ideal circumstances and response prediction. The coefficients of measurements ( $R^2 = 0.9899$  and  $R^2 = 0.9798$ , respectively), which are values that reflect the amount of departure from the mean, were used to express the adequacy of the polynomial equation for % EE and PS. A strong correlation among the experimental and theoretical data can be used to explain the high adjusted  $R^2$  values (Fig. 1a, b). Both figures demonstrate the normal distribution of mean-centered errors, the linear correlation responses to variables, and the consistency between theoretical and experimental results (Abd-El-Aziz

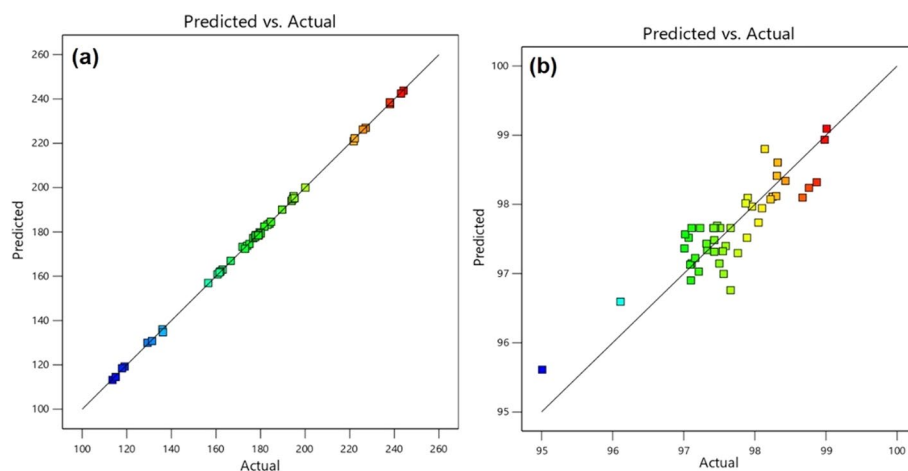


**Fig. 1** **a** The actual vs. predicted data of controlled PS (nm) and **b** the actual vs. predicted data of controlled EE (%)

et al. 2022). Regression analysis of BBD was used to assess the data and enable the development of mathematical models for PS (nm) and % EE.

#### PS of SLNs

According to research, the QuR-SLNs' approximate PS fall between 113.63 and 244.13 nm. Equation (3) represents the equation of regression for the PS in relations of coded factors:

$$\text{PS} = +178.49 + 53.86X_1 - 5.35X_2 + 11.42X_3 + 6.18X_4 + 10.10X_5. \quad (3)$$

PS has grown by boosting the  $X_1$ ,  $X_2$ , and  $X_4$ , as shown in Eq. (3). The dispersion gets more viscous as the lipid ratio rises, meaning that any shear pressure applied would not be sufficient to reduce size but rather would result in the achievement of a higher size (Taherzadeh et al. 2021). In addition, if there was not enough surfactant to coat the surface of the particles, the larger lipid content may cause the PS to increase. As a result, the content, type, and degree of surfactants affect the stability and PS of nanoparticles. In this study, ratios of 10:90 were chosen to study Span and Tween 80. The hydrophilic–lipophilic balance (HLB) rate with surfactant and co-surfactant structure may have an impact on the outcomes. With a 90:10 ratio, the bulk lipids (SA and TpN) must have an HLB value of 14.94. Based on “required value,” the mixture of tween80:span80 (90:10) was required to add to the system (Fang et al. 2022). Since the drug amount has a negative coefficient, increasing the drug amount will increase the PS. This impact also showed a significant effect on this research ( $p < 0.05$ ). It might be due to the addition of QuR into the main principle of nanoparticles with subsequently increased PS. Sonication time ( $X_4$ ) showed that PS significantly increased with increase in sonication time ( $X_4$ ); these observations should be predictable. More aggregation, particle contact, size enlargement, and decreased surface area were all effects of longer sonication times (Yang et al. 2021). Moreover, sonication only serves to emulsify lipids in the aqueous phase in this stage. This process was an intermediary one that did not result in the final particles. Figure 2a–d can be used to assess how independent variables affect PS.

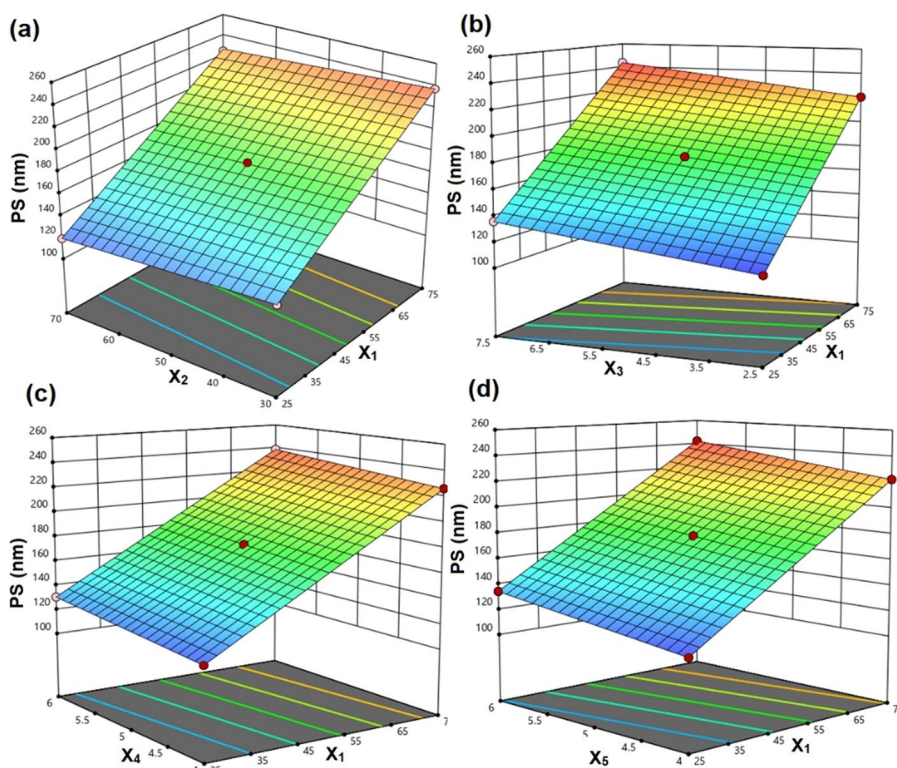


**Fig. 2** a–d 3D response surface plot of the  $(2^{5-1})$  BBD of PS (nm)

**% EE of SLN**

The polynomial quadratic equation of the estimated % EE and presented relation to coded components is shown in Eq. (4):

$$\begin{aligned}
 \text{EE (\%)} = & +97.66 - 0.3063X_1 + 0.2175X_2 + 0.0387X_3 \\
 & - 0.1594X_4 + 0.3856X_5 - 0.2300X_1X_2 - 0.7975X_1X_3 \\
 & - 0.4325X_1X_4 + 1.36X_1X_5 - 0.2575X_2X_3 \\
 & - 0.2850X_2X_4 + 0.3425X_2X_5 + 0.5600X_3X_4 \\
 & - 0.0100X_3X_5 + 0.0850X_4X_5.
 \end{aligned}
 \tag{4}$$

In a coded equation, enormous positive coefficients often designate that decreasing the variable value is desired, and vice versa, that increasing the variable value would enhance the response. The magnitudes of the coefficients show how much each component contributed to the response in relation to the other. The EE of a lipophilic agent like QuR into SLNs is high, as shown in Table 1. The high EE in all formulations, which ranged from 95.01 to 99.01%, can be attributed to the lipid structure’s important involvement in QuR incorporation. Overall, high EE was the result of high solubility of the QuR in the melted lipid and provided more and more spare to accommodate excessive drugs. The high crystallinity of TpN and the high crystalline order of the nanoparticles may have contributed to the increased entrapment effectiveness of QuR seen in the low ratios of TpN compared to SA (Naseri et al. 2015).

The % EE reduced as the sonication duration was extended because more particles in the aqueous and lipid phases interacted with one another and the drug exited the

lipid core. Surfactant ratios have a considerable impact on the substance’s solubility in the superficial phase because the lipophilic nature of QuR molecule was trapped in the lipid matrix core, but in this study, the effects were not found to be particularly significant. Variables’ impact on a reaction can be assessed by looking at the response graphs shown in Fig. 3a–d.

**Optimization**

After computing the polynomial equations, the desirability function (DF) was utilized to interpret the dependent and independent variables in STATISTICA software to control the variables’ optimal levels as they relate to the PS and EE% of SLNs. The DF contains 0, 0.5, and 1 of 3 inflection points and depends on a precise prediction of the DF, and eight measurable replies, eight qualitative responses, and a combination of both were achieved after a single measurement. First, the response was transformed into a specific desirability function that ranges from 0 to 1. As previously discussed, a value of 1 or 0 corresponds to a preferred or undesired circumstance, respectively. The profile for predicted values and DF in the STATISTICA 7.0 software was used for the optimization process. According to the BBD design matrix, the highest and lowest yields depend on the DF of corresponding dependent variable on the PS and EE% as displayed in Table 2.

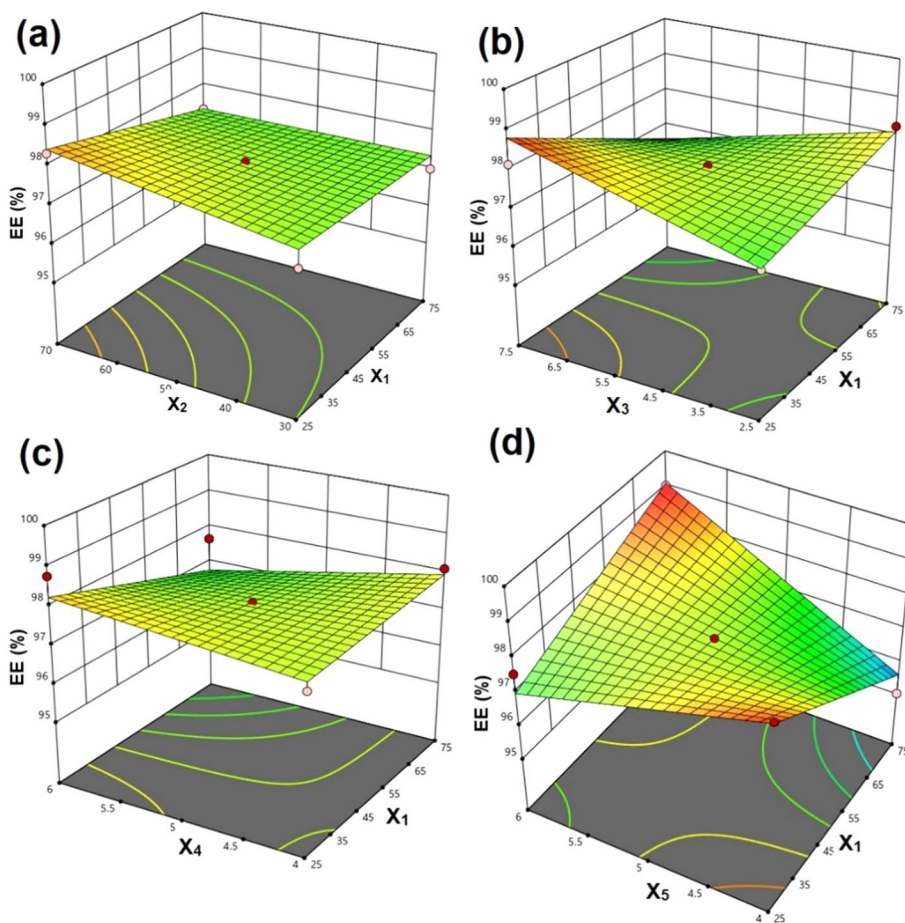


**Fig. 3.** 3D response surface plot for the  $(2^{5-1})$  BBD of EE (%) (a–d)

By increasing entrapment efficacy and lowering PS, the values for the optimal factors were found. These calculations and the desirability function were used to optimize the EE% and PS of the SLNs to  $97.8 \pm 1.16\%$  and  $132.16 \pm 4.1$  nm respectively, at the ideal values of the following variables: SA/TpN ratio (90/10), Tween 80/Span 80 ratio (10/90), lipid/drug ratio (3 ppm), sonication time (4 min), and homogenization time (5 min). According to the ideal levels of formulation factors, the anticipated model for the new batch of SLN was formulated. The experiential optimized preparation has an EE (%) of  $97.68 \pm 0.28$  and a PS of  $129.1 \pm 3.6$  nm in size; this outcome was reasonably consistent through the expected results. The accuracy of the BBD used to forecast a desirable SLN formulation can be seen by comparing these observed outcomes to theoretical predictions.

### Shape and morphology

Figure 4a depicts the morphology of freshly prepared B-SLN. Owing to the nature (adhesiveness) of the polymer, it exhibited irregularly presented rough particle form with a thick lipid matrix that was somewhat aggregated. SEM was used to examine the QuR-SLNs' shape and surface morphology (which was chosen as the best formulation). The QuR-SLN's smooth surface morphology is shown in Fig. 4a, b. The micrographs showed a smooth surface and a semi-spherical form.

### DSC

The DSC thermogram of the principal constituents QuR, SA, and TpN and the samples of QuR-SLN are shown in Fig. 5a. QuR showed a strong peak in its crystallinity at  $324.09$  °C, which is also its melting point. Whereas crystalline endothermic peak of QuR vanished on DSC thermograms of blank SLN and QuR-SLNs, they do have an endothermic peak around the melting point of SA. The outcomes demonstrated that the lipid matrix of the SLN completely dissolved the QuR. Blank-SLNs displayed a wide-ranging endothermic peak at  $67.8$  °C in contrast to QuR-SLNs, which displayed a wide-ranging  $61.3$  °C of endothermic peak. This modest change in peak was most likely brought on by QuR assimilation within the lipid matrix (Vijayakumar et al. 2017).

### XRD

Figure 5b displays the XRD pattern of bulk lipids (SA and TpN), free QuR, SLN, and QuR-SLNs. The XRD findings corroborated the conclusions reached by the DSC

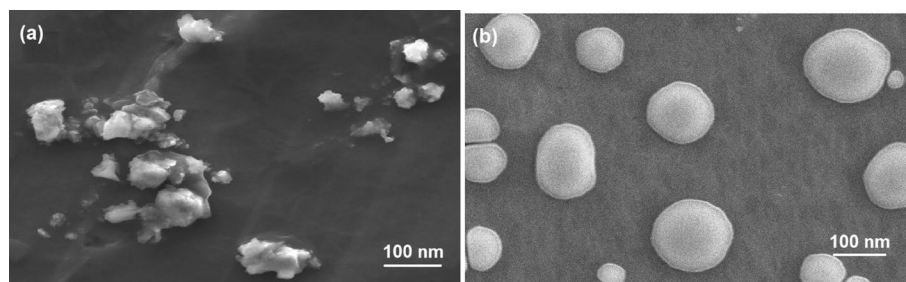


**Fig. 4** SEM image of **a** B-SLN and **b** QuR-SLN

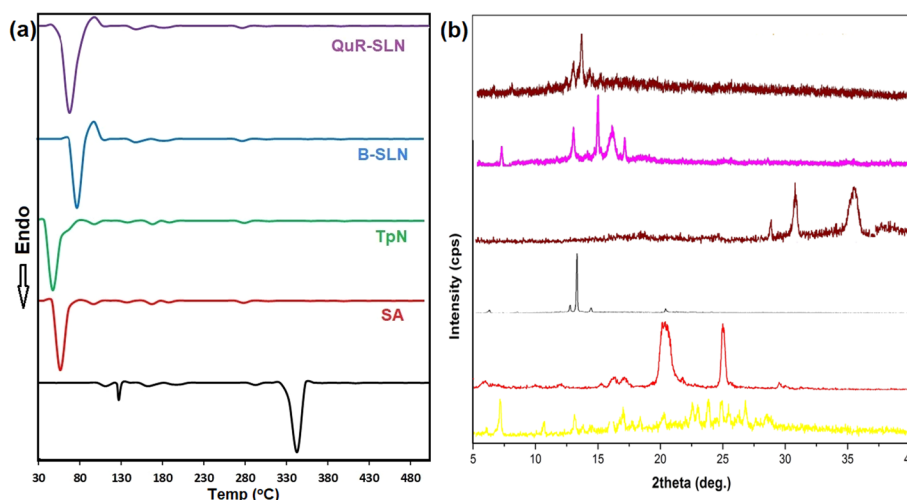


**Fig. 5** **a** DSC thermogram and **b** XRD pattern of QuR, PEG 5000, SA, TpN, B-SLN, and QuR-SLN

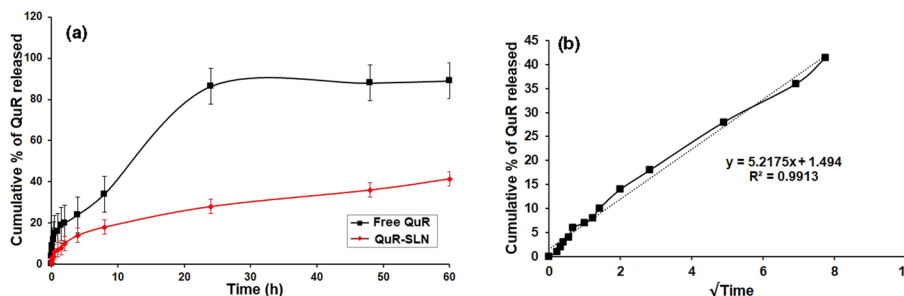


**Fig. 6** Cumulative % of QuR release from QuR-SLN and **b** Higuchi model kinetic release of QuR-SLN ( $\sqrt{T}$  vs. time); (mean  $\pm$  SD,  $n = 3$ )

investigation. The two prominent strong peaks at  $2\theta$  of  $7^\circ$  and  $18.9^\circ$  in the QuR diffraction pattern could not be seen in the diffractogram of QuR-SLNs, indicating that the QuR was dissolved inside the lipid lattice of the QuR-SLNs in a stable amorphous form. In addition, the XRD spectra among  $2\theta$  angles at  $11^\circ$  and  $18^\circ$  in SLNs were less intense than those in bulk lipid, confirming lower lipid matrix crystallinity relative to bulk solid lipid and a less organized lipid matrix in SLNs. Furthermore, examining the diffraction patterns did not show much difference in the pattern between drug-free SLNs and SLNs that contained QuR, suggesting that the presence of QuR did not alter the character of SLNs. This outcome can be explained by the fact that QuR was trapped in the lipid core of SLNs (Hazra et al. 2015). In addition, compared to the SLNs, the initial abrupt peak in the QuR-SLNs similarly exhibited a little lower intensity.

### In vitro QuR release

This study tested the in vitro release of QuR from SLNs over a 60-h period at  $37^\circ\text{C}$  using a dialysis bag (Fig. 6a). The PBS showed a pH of 6.8 when 50% v/v of ethanol was added due to the limited water solubility of QuR. Our findings indicated that over the test period, up to  $41.12 \pm 1.6\%$  of the drug payload was released, contributing to the free drug ( $86.67 \pm 4.23\%$ ). After 12 h, the release of SLNs was delayed and decreased,

which can be attributed to the slower diffusion of QuR through diffusion and dissolution mechanisms due to the SLN's inner solid matrix core. Although the release rate of SLNs could be influenced by factors such as high diffusion coefficient, and large surface area, however, the small molecular size or low viscosity predominated the influence on the matrix system (Jamal Moideen et al. 2020). In this research, the release profiles of SLN and free QuR were evaluated.

In addition, the following Higuchi kinetic equation was used to assess the release data:  $Qt = kt^{0.5}$  where  $k$  is the constant of release rate and  $Qt$  is the amount of QuR released at time  $t$ . It was discovered that the protracted release characteristic of QuR, as it has been reported for QuR-SLMN, was well matched to Higuchi square root model with regard to the release model of all preparations (Fig. 6b). The release profile of QuR as of homogeneous and granular matrix systems was fitted linearly, proving that it is diffusion controlled (Manju and Sreenivasan 2012). Kinetics are shown by the  $R^2$  value of the in vitro release values, and the  $K$  values, or release rate constant, are calculated using the Higuchi model plot.

**Determination of  $IC_{50}$**

The QuR-SLN had greater cytotoxic action than free QuR and QuR-SLN, according to the MTT test data. According to Manju and coworkers, this may be because differences in the cellular absorption profile enable the QuR-SLN to function more effectively. According to the assay findings, QuR-SLN has increased cytotoxicity and can deliver the drug to Caco-2 cells with efficiency. It does this by actively targeting the cells through the endocytic process (Paranthaman et al. 2022). When cytotoxicity is present in higher concentrations, cell viability declines; nevertheless, QuR-SLN performed substantially better than free QuR. The  $IC_{50}$  values for QuR-SLN were measured around 49  $\mu\text{M}/\text{mL}$ , in the cytotoxic findings of the MTT-reduction experiment on Caco-2 cell line (Fig. 7), whereas the value for free QuR was found to be 128  $\mu\text{M}/\text{mL}$  for 24 h.

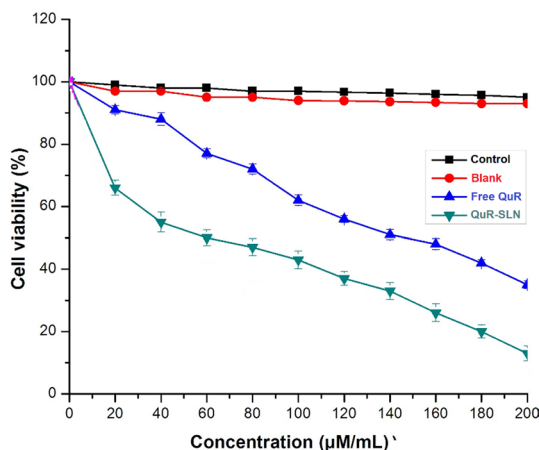


**Fig. 7** The effect of control, blank, free QuR, and QuR-SLN in vitro cytotoxicity on Caco-2 cell line (mean ± SD,  $n = 3$ )

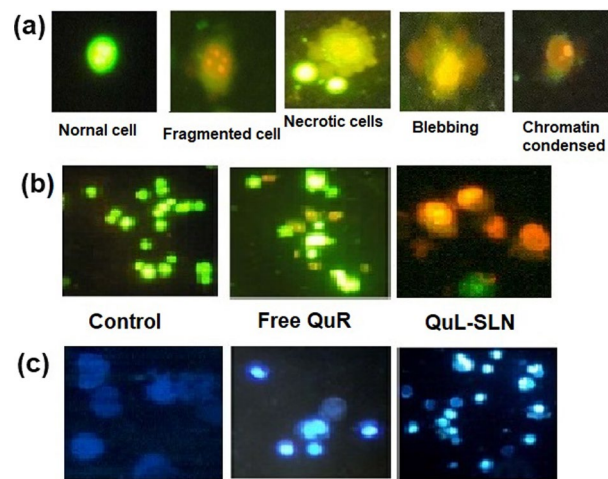


**Fig. 8** Morphology of Caco-2 cells **a** Various apoptotic morphologies of Caco-2 cells on **b** AO/EB and **c** Hoechst staining visualized under fluorescent microscope of control, free QuR, and QuR-SLN. Clear picture

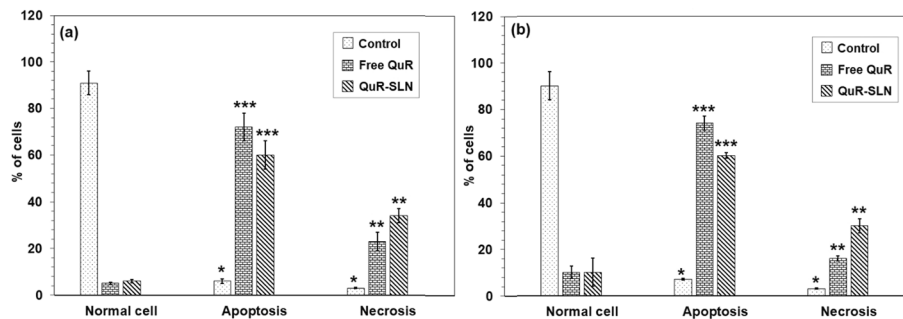


**Fig. 9** Percentage of normal, apoptotic, and necrotic cells after 24 h treatment with **a** AO/EB staining and **b** Hoechst staining. Significant deviations from the control are denoted by \*\*\* $p < 0.001$  and \*\* $p < 0.05$ , according to the Student's *t* test results

### Cell death observation

#### AO/EB staining

To demonstrate the apoptotic morphologies brought on by QuR-SLN, AO/EB dual staining were used. Three different types of cytological changes were identified based on the morphological characteristics of nuclei (Fig. 8a). Necrotic cells had limited chromatin condensation or fragmentation, were orange-to-red shining nuclei, and were swollen. Late apoptotic cells had compressed or fragmented chromatin as well as orange-to-red fluorescing nuclei. As shown in Fig. 8a, they largely contained the second late apoptotic cell deaths. The morphological alterations shown by this staining technique show that the cells were destroyed by both necrosis and apoptosis after being exposed to QuR-SLN for 24 h (Chen et al. 2020). However, as shown in Fig. 8b, a significant portion of cells died by the apoptotic process as opposed to necrosis (Fig. 9a).

### **Hoechst staining**

Apoptosis is characterized by DNA damage, chromatin marginalization and condensation, membrane cell thinning and blebbing, and cell death into apoptotic figures that are phagocytosed by macrophages (Chen et al. 2020).

Hoechst staining has been suggested as a key method for determining apoptosis. After the cells had been exposed to QuR-SLN at the  $IC_{50}$  concentration for 24 h, the cells were examined for significant cytological changes. The treated cells displayed late apoptosis-related dot-like chromatin (Fig. 8c) as well as the microscopic cytological changes linked to apoptosis that were previously discussed. However, a few cells exhibited symptoms of necrotic death. The amounts of healthy and sick cells computed in the control and QuR-SLN-treated groups are shown in Fig. 9b.

### **Conclusion**

The QuR-SLNs have been prepared in the current work, and optimization of an SLN preparation was a complex procedure that necessitates taking into account a significant number of variables and how they interact with one another. This study unequivocally proves that the Box–Behnken design may be used to successfully produce the optimal formulations. The values of chosen independent variables can be predicted using the generated polynomial equations and response surface plots to prepare the best formulations with the desired features. These SLNs have a spherical shape and a uniform size distribution via SEM analysis. QuR was discovered to be in an amorphous state in SLNs using solid-state research. In aqueous media, the produced SLN release profile was examined. It revealed sustained release over the course of 48 h, with up to  $41.12 \pm 1.6\%$  release. The in vitro cytotoxicity assay was utilized at a concentration of  $49 \mu\text{M}/\text{mL}$  to evaluate the inhibition of cell growth at different concentrations and the  $IC_{50}$ . The morphology of cell death via apoptosis was found in the Caco-2 cells. After testing, it was discovered to have less necrosis and to be very effective at eliminating cancer cells.

### **Author contributions**

All authors contributed substantially to the body of work. JMMM, FA, ME-S, MAAM, MBE, AFD, and AMI: conceptualization, methodology, software, formal analysis, writing—original draft preparation. JMMM and KV: writing—review and editing. AEI and YBAA: data curation, methodology, software, writing—review and editing. JMMM and SED: supervision, project administration, and funding acquisition.

### **Funding**

Open Access funding enabled and organized by Projekt DEAL. This research was funded by Princess Nourah bint Abdulrahman University Researchers Supporting Project number (PNURSP2023R110), Princess Nourah bint Abdulrahman University, Riyadh, Saudi Arabia and by the Researchers Supporting program, AlMaarefa University, Riyadh, Saudi Arabia. Also, the work supported via funding from Prince Sattam bin Abulaziz University project number (PSAU/2024/R/1445), Riyadh, Saudi Arabia. The authors extend their sincere appreciation to the Deanship of Scientific Research at King Khalid University for funding this study through the Large Research Group Project under grant number "RGP 2/109/44".

### **Availability of data and materials**

All data are available from the corresponding author upon reasonable request.

### **Declarations**

#### **Ethics approval and consent to participate**

Not applicable.

#### **Consent for publication**

Not applicable.

### Competing interests

The authors declare that they have no conflict of interest.

### Author details

<sup>1</sup>Faculty of Pharmacy & BioMedical Sciences, MAHSA University, Bandar Saujana Putra, 42610 Jenjarom, Selangor, Malaysia. <sup>2</sup>Department of Anesthesia Technology, College of Applied Medical Sciences in Jubail, Imam Abdulrahman Bin Faisal University, P.O. Box 4030, Dammam, Saudi Arabia. <sup>3</sup>Department of Basic Medical Sciences, College of Medicine, AlMaarefa University, P.O. Box 71666, 11597 Riyadh, Saudi Arabia. <sup>4</sup>Department of Anatomy, Faculty of Medicine, Mansoura, Egypt. <sup>5</sup>College of Applied Medical Sciences, King Saud bin Abdulaziz University for Health Sciences, Al-Ahsa, Saudi Arabia. <sup>6</sup>King Abdullah International Medical Research Center, Al-Ahsa, Saudi Arabia. <sup>7</sup>Department of Pharmacology, College of Pharmacy, King Khalid University, Abha, Asir, Saudi Arabia. <sup>8</sup>College of Pharmacy and Nursing, University of Nizwa, Birkat Al Mauz, 616 Nizwa, Oman. <sup>9</sup>Natural and Medical Sciences Research Center, University of Nizwa, Birkat Al Mauz, 616 Nizwa, Oman. <sup>10</sup>Department of Basic Medical Sciences, College of Medicine, Princess Nourah bint Abdulrahman University, P.O. Box 84428, 11671 Riyadh, Saudi Arabia. <sup>11</sup>Department of Nursing, College of Applied Medical Sciences, Prince Sattam bin Abdulaziz University, 11942 Al-Kharj, Saudi Arabia. <sup>12</sup>Department of Family and Community Health Nursing, Faculty of Nursing, Port Said University, Port Fouad, Egypt. <sup>13</sup>Institute of Medicinal and Pharmaceutical Chemistry, Technische Universität Braunschweig, Braunschweig, Germany.

Received: 2 January 2024 Accepted: 22 January 2024

Published online: 26 February 2024

### References

- Abd-El-Aziz NM, Hifnawy MS, El-Ashmawy AA, Lotfy RA, Younis IY (2022) Application of Box–Behnken design for optimization of phenolics extraction from *Leontodon hispidulus* in relation to its antioxidant, anti-inflammatory and cytotoxic activities. *Sci Rep* 12(1):8829
- Chen S-Q, Wang C, Song Y-Q, Tao S, Yu F-Y, Lou H-Y, Hu F-Q, Yuan H (2020) Quercetin covalently linked lipid nanoparticles: multifaceted killing effect on tumor cells. *ACS Omega* 5(46):30274–30281
- Das SS, Hussain A, Verma PRP, Imam SS, Altamimi MA, Alshehri S, Singh SK (2020) Recent advances in liposomal drug delivery system of quercetin for cancer targeting: a mechanistic approach. *Curr Drug Deliv* 17(10):845–860
- David AVA, Arulmoli R, Parasuraman S (2016) Overviews of biological importance of quercetin: a bioactive flavonoid. *Pharmacogn Rev* 10(20):84
- El-Hela AA, Bakr MSA, Hegazy MM, Dahab MA, Elmaaty AA, Ibrahim AE, El Deeb S, Abbass HS (2023) Phytochemical characterization of *Pterocephalus frutescens* with in-silico evaluation as chemotherapeutic medicine and oral pharmacokinetics prediction study. *Sci Pharm* 91(1):7
- Fang Q, Zhao X, Li S, Qiu Z, Wang Z, Geng Q (2022) Effect of surfactants with different hydrophilic–lipophilic balance on the cohesive force between cyclopentane hydrate particles. *J Mar Sci Eng* 10(9):1255
- Gao W, Hu C-MJ, Fang RH, Zhang L (2013) Liposome-like nanostructures for drug delivery. *J Mater Chem B* 1(48):6569–6585
- Greenland S, Senn SJ, Rothman KJ, Carlin JB, Poole C, Goodman SN, Altman DG (2016) Statistical tests, P values, confidence intervals, and power: a guide to misinterpretations. *Eur J Epidemiol* 31:337–350
- Hazra M, Mandal DD, Mandal T, Bhuniya S, Ghosh M (2015) Designing polymeric microparticulate drug delivery system for hydrophobic drug quercetin. *Saudi Pharm J* 23(4):429–436
- Jacob S, Nair AB, Shah J, Gupta S, Boddu SH, Sreeharsha N, Joseph A, Shinu P, Morsy MA (2022) Lipid nanoparticles as a promising drug delivery carrier for topical ocular therapy—an overview on recent advances. *Pharmaceutics* 14(3):533
- Jamal Moideen MM, Alqahtani A, Venkatesan K, Ahmad F, Krisharaju K, Gayasuddin M, Shaik RA, Ibraheem KMM, Salama MEDM, Abed SY (2020) Application of the Box–Behnken design for the production of soluble curcumin: skimmed milk powder inclusion complex for improving the treatment of colorectal cancer. *Food Sci Nutr* 8(12):6643–6659
- Kumar R, Singh A, Garg N, Siril PF (2018) Solid lipid nanoparticles for the controlled delivery of poorly water soluble non-steroidal anti-inflammatory drugs. *Ultrason Sonochem* 40:686–696
- Lotfi N, Yousefi Z, Golabi M, Khalilian P, Ghezellbash B, Montazeri M, Shams MH, Baghbadorani PZ, Eskandari N (2023) The potential anti-cancer effects of quercetin on blood, prostate and lung cancers: an update. *Front Immunol* 14:1077531
- Manju S, Sreenivasan K (2012) Gold nanoparticles generated and stabilized by water soluble curcumin–polymer conjugate: blood compatibility evaluation and targeted drug delivery onto cancer cells. *J Colloid Interface Sci* 368(1):144–151
- Mármol I, Sánchez-de-Diego C, Pradilla Dieste A, Cerrada E, Rodríguez Yoldi MJ (2017) Colorectal carcinoma: a general overview and future perspectives in colorectal cancer. *Int J Mol Sci* 18(1):197
- Michalkova R, Mirossay L, Kello M, Mojzisoava G, Baloghova J, Podracka A, Mojzis J (2023) Anticancer potential of natural chalcones: in vitro and in vivo evidence. *Int J Mol Sci* 24(12):10354
- Mohamed JM, Alqahtani A, Ahmad F, Krishnaraju V, Kalpana K (2021a) Pectin co-functionalized dual layered solid lipid nanoparticle made by soluble curcumin for the targeted potential treatment of colorectal cancer. *Carbohydr Polym* 252:117180
- Mohamed JMM, Ahmad F, Alqahtani A, Raju VK, Anusuya M (2021b) Studies on preparation and evaluation of soluble 1:1 stoichiometric curcumin complex for colorectal cancer treatment. *Trends Sci* 18(24):1403–1403
- Muthu Mohamed JM, Kavitha K, Ahmad F, Sherbiny ME, Ebrahim D, El-Sagheer AM, Ebrahim HA, Abdelmonem Elsherbini DM, Ebrahim Abdelrahman MA, Dejene M (2022) Curcumin plant for colorectal cancer prediction and prevention using in silico molecular analysis; HOT-MELT extrusion. *Evid Based Complement Alternat Med*. <https://doi.org/10.1155/2022/4376960>

- Naseri N, Valizadeh H, Zakeri-Milani P (2015) Solid lipid nanoparticles and nanostructured lipid carriers: structure, preparation and application. *Adv Pharm Bull* 5(3):305
- Paranthaman S, Uthaiyah CA, Osmani RAM, Hani U, Ghazwani M, Alamri AH, Fatease AA, Madhunapantula SV, Gowda DV (2022) Anti-proliferative potential of quercetin loaded polymeric mixed micelles on rat C6 and human U87MG glioma cells. *Pharmaceutics* 14(8):1643
- Rahman N, Sameen S, Kashif M (2019) Application of Box–Behnken design and desirability function in the optimization of spectrophotometric method for the quantification of WADA banned drug: acetazolamide. *J Mol Liq* 274:270–277
- Rawla P, Sunkara T, Barsouk A (2019) Epidemiology of colorectal cancer: incidence, mortality, survival, and risk factors. *Gastroenterol Rev/przegląd Gastroenterologiczny* 14(2):89–103
- Roy H, Panda SP, Panda SK, Tripathi AK, Srivastava SK, Nayak BS, Singh PK, Singh GD (2023) *N*-Trimethyl chitosan and tripalmitin loaded solid lipid nanoparticles of tofacitinib citrate: characterization and in-vivo anti-inflammatory assessment. *J Drug Deliv Sci Technol* 87:104789. <https://doi.org/10.1016/j.jddst.2023.104789>
- Satheesh V, Mohamed JMM, El-Sherbiny M, Othman G, Al-Serwi RH, Thilagar S (2022) Sunlight-assisted green synthesis of silver nanoparticles using *Zizania latifolia* extract: toward antimicrobial applications. *Biomass Convers Biorefin.* <https://doi.org/10.1007/s13399-022-03363-7>
- Tahezadeh S, Naeimifar A, Yeganeh EM, Esmaili Z, Mahjoub R, Javar HA (2021) Preparation, statistical optimization and characterization of propolis-loaded solid lipid nanoparticles using Box–Behnken design. *Adv Pharm Bull* 11(2):301
- Vijayakumar A, Baskaran R, Jang YS, Oh SH, Yoo BK (2017) Quercetin-loaded solid lipid nanoparticle dispersion with improved physicochemical properties and cellular uptake. *AAPS PharmSciTech* 18:875–883
- Yadav K, Yadav D, Kumar S, Narra K, El-Sherbiny M, Al-Serwi RH, Othman G, Sendy JS, Mohamed JMM (2022) Natural biodegradable and polymeric nanoparticles for the delivery of nescapine for cancer treatment. *Biomass Convers Biorefin.* <https://doi.org/10.1007/s13399-022-03334-y>
- Yang G, Lin W, Lai H, Tong J, Lei J, Yuan M, Zhang Y, Cui C (2021) Understanding the relationship between particle size and ultrasonic treatment during the synthesis of metal nanoparticles. *Ultrason Sonochem* 73:105497

### Publisher's Note

Springer Nature remains neutral with regard to jurisdictional claims in published maps and institutional affiliations.